The Ti_2CO_2 MXene as a nucleobase 2D sensor: a first-principles study

José D. Gouveia[a,*], Gerard Novell-Leruth[a], Francesc Viñes[b], Francesc Illas[b], José R. B. Gomes[a,*]

[a] *CICECO – Aveiro Institute of Materials, Department of Chemistry, University of Aveiro, Campus Universitário de Santiago, Aveiro, Portugal*

[b] *Departament de Ciència de Materials i Química Física & Institut de Química Teòrica i Computacional (IQTCUB), Universitat de Barcelona, c/ Martí i Franqués 1, 08028 Barcelona, Spain*

*Corresponding authors: E-mails: gouveia@ua.pt ; jrgomes@ua.pt

Abstract

MXenes are a recently discovered class of two-dimensional materials, which have been attracting much interest by virtue of their promising biomedical and electronic applications. Here, we report on the results of first-principles calculations, based on density functional theory (DFT) including dispersion, of the adsorption energies and configurations of the five nucleobases, molecules conforming nucleotides in nucleic acids, such as DNA and RNA, on the oxygen-terminated titanium carbide MXene surface (Ti_2CO_2), chosen as a prototype MXene due to titanium being the most biocompatible transition metal. We find that physisorption is the most likely mechanism of adsorption on the Ti_2CO_2 (0001) basal surface, with the molecules sitting parallel to the MXene, about 2.5 Å away. The calculated adsorption energies and Bader charge transfer values are moderate, as desired for sensing applications. We find a fair correlation between the adsorption energies and the van der Waals volumes of the nucleobases, hinting towards an adsorption dominated by van der Waals interactions. No structural deformation is observed on the molecules or on the surface. Thus, all of our conclusions support the potential applicability of the Ti_2CO_2 MXene as a suitable nucleobase sensor.

Introduction

Deoxyribose nucleic acid (DNA) and ribonucleic acid (RNA) are macromolecules contained in, and used by, all living cells and all forms of life on Earth. DNA is a double helix molecule, twisted like a spiral staircase, whose railings, often called the *backbone*, are alternating deoxyribose sugar-phosphate chains. Each step of the staircase consists of two hydrogen-bonded molecules called nucleobases. Four distinct nucleobases can be found in DNA: adenine (A), cytosine (C), guanine (G), and thymine (T). All nucleobases are based on aromatic heterocyclic organic rings. A and G are called the *purine nucleobases*, as their structures derive from purine, a double-ring compound, and C and T are *pyrimidine nucleobases*, due to their resemblance to pyrimidine. Every step of the DNA staircase contains a purine-pyrimidine base pair —either A-T or C-G—, with the molecules connected by a double or triple hydrogen bond, respectively. This manner of nucleobase pairing ensures that all steps of the staircase have approximately the same width, thus contributing to the stability of the DNA double helix. Nucleobases are the building blocks of DNA and RNA, just as amino acid sequences form proteins. Each different sequence of nucleobase pairs encodes the genetic information of a unique life form and, in general, living beings translate every three nucleobase pairs into a single amino acid, as per the genetic code. An intermediate compound, ribonucleic acid (RNA), is formed before this translation occurs. The structure of RNA is very similar to that of DNA, with three key differences. First, as its name suggests, the backbone of the former contains ribose rather than deoxyribose. Second, RNA is often a single chain of nucleobases, rather than a double helix. Lastly, when transcribing portions of DNA into RNA, all DNA nucleobases are replaced by their corresponding bases, except for T, which is replaced by uracil (U), a pyrimidine nucleobase [1]. Given the central role of DNA and RNA in all sorts of metabolic related processes, their sensing and nucleobases sequence recognition are key in future applied studies, ranging from disease prevention to improved therapies. A nucleobase sensor, apart from being able to recognize the different components under *in vivo* conditions, should be hydrophilic and compatible with the cytosol medium in cells. Thus, at the end of the day, sensing is an applied surface science issue, where two-dimensional (2D) large-surface-area materials are appealing options fostering the DNA/RNA contact, even permitting the sensing of small molecular concentrations.

MXenes are a family of 2D materials, first reported in 2011 [2], with details on their synthesis and basic properties described in a recent review [3]. MXenes are made up of a few atomic layers of transition metals —the M element— alternated with layers of nitrogen or carbon —the X element, usually arranged in an face-centered cubic stacking, surrounded by outer terminating layers (T), whose composition depends on the synthesis method (often O, OH, F, or H), with stoichiometry $M_{n+1}X_nT_x$ [4]. MXenes are known for their high conductivity, oxidation resistance and surface area, as well as hydrophilicity and easily tunable surface termination [4–6]. Their suitability encompasses energy storage applications [6–8], carbon capture technologies [9–11], heterogeneous catalysis [12–14], and bio-sensing [15], among many others. Titanium carbide $Ti_{n+1}C_n$ MXenes are among the most studied for biomedical applications, since titanium is the most biocompatible transition metal [16]. In this work, we focus on the bio-molecule sensing capabilities of the oxygen-terminated three-layered titanium carbide MXene, Ti_2CO_2, as this particular termination is one of the most commonly found when synthesizing MXenes under oxidative environments. The Ti_2CO_2 MXene has been experimentally [17] demonstrated as an amino acid (arginine) sensor via adsorption, and DNA transport studies indicate that these surfaces can be used for DNA translocation and sensing [18]. Moreover, earlier theoretical studies predict that titanium carbide MXenes should be

suitable as sensors for twenty of the proteinogenic amino acids [19,20]. Indeed, the results of one of our previous works, carried out to evaluate the suitability of a titanium carbide MXene as an amino acid sensor [19], suggested that amino acids exothermically adsorb on Ti_2CO_2 with moderate adsorption energies, ideal for molecule sensing, as an excessively strong adsorption would cause the surface to become contaminated by the sensed molecule, even potentially irreversibly deformed, after long exposure.

In general, the most recent theoretical reports on nucleobase adsorption on different surfaces present adsorption energies and charge transfer values of the same order, and sorted along the van der Waals volumes of the molecules. The surfaces scrutinized so far include MoS_2 surfaces [21], boron sheets [22], penta-graphene [23], silicene [24], and tellurene [25]. In the case of MoS_2, models with an added single atom of a different chemical element predicted that the adsorption can be strengthened by surface doping. In particular, on Li-doped MoS_2 the adsorption of nucleobases becomes around 0.7 eV stronger, up to -1.80 eV [21]. The same happens on Si-doped MoS_2, where the nucleobase adsorption energies were estimated to go up to -3.16 eV [26]. In these two cases, the chemisorption was deemed unsuitable for sensing, as desorption would be severely hindered, and the surface would become irreversibly poisoned. On the other hand, dopants like P, Cl, or Se lead to adsorption strength barely over -1 eV. According to a theoretical report on nucleobase adsorption on germanane, the adsorption energies on this surface go up to -1.25 eV and follow the order T > U > G > C > A, which is very distinct from the one found for all other materials [27].

The aforementioned results serve as motivation for the present work, where we assess the suitability of the Ti_2CO_2 MXene as a nucleobase sensor. Theoretically, this can be studied using electronic structure methods, by calculating the adsorption energy and Gibbs free energy of adsorption of a single nucleobase. Density functional theory (DFT) is a convenient theoretical framework providing an efficient computational tool that can be employed to address this subject. In fact, DFT is broadly used in all sort of surface science and computational heterogeneous catalysis and, in particular, has been used to perform similar studies for amino acids on different families of surfaces [19,28,29], where it was additionally established that a realistic description of the adsorption process requires the inclusion of dispersion corrections to the total energies. As a result, in the present work, we study the individual adsorption of the five nucleobases on Ti_2CO_2 based on DFT calculations. The rest of this paper consists of a description of the computational details of our calculations, then a presentation of their results, and finally a summary of our conclusions.

Computational methods

The general computational setup used in this work closely resembles that of a previous similar study of ours [19]. Briefly, the calculations were performed using the VASP package [30–33]. The Perdew-Burke-Ernzerhof (PBE) exchange-correlation functional [34] with D3 dispersion corrections [35,36] was chosen, as it has been shown to correctly describe adsorption phenomena on MXenes, which are dominated by van der Waals interactions [11,13,14,19,37,38]. The effect of core electrons on the valence electron density was implicitly treated by employing the projector-augmented wave (PAW) method. For each chemical element involved in this work, the valence electrons explicitly considered are as follows: Ti (d^2s^2), C (s^2p^2), O (s^2p^4), N (s^2p^3), H (s^1). Convergence tests, aiming to obtain relative energies converged within 1 meV/atom, revealed that spin polarization does not change any result, as expected from the nature of the interaction. In all calculations, a plane-wave (PW) basis set with an energy cutoff of 400 eV was used to solve the Kohn-Sham equations, while the total energies were converged within 10^{-7} eV. During atomic position relaxation, the structures were considered optimized when the maximum force acting on every atom became smaller than 0.005 eV/Å. The Brillouin zone sampling was carried out using a Γ-centered 2×2×1 grid of **k**-points [39].

To model the Ti_2CO_2 MXene (0001) basal surface, a rhombic supercell was considered, with periodic boundary conditions in all cartesian directions, see Fig. 1. This supercell contained a *p*(5×5) grid of Ti_2CO_2 unit cells —accounting for a total of 125 atoms—, separated by approximately 15.5 Å of vacuum width in order to avoid interaction between supercell replicas in the direction perpendicular to the surface, even when a nucleobase molecule is adsorbed. The calculated lattice constant and MXene width, $a = 3.015$ Å and $d = 4.46$ Å, respectively, are in excellent agreement with the corresponding values obtained at the same level of theory by other authors [40].

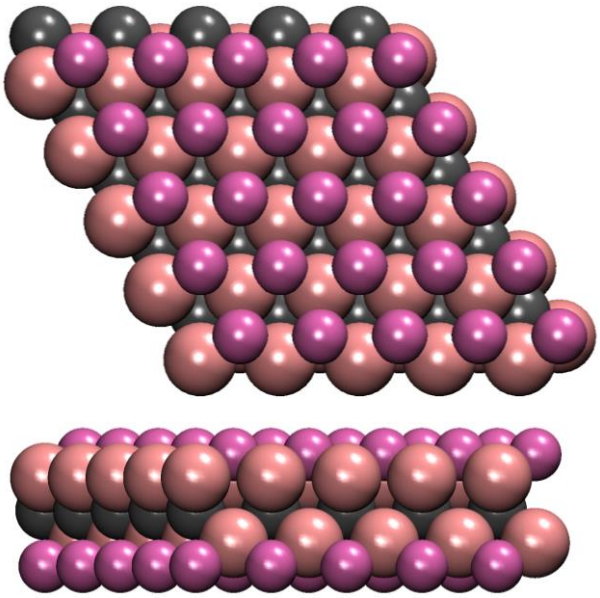

Fig. 1. Top (top image) and side (bottom image) views of the Ti_2CO_2 *p*(5×5) supercell. The spheres represent atoms of color-dependent chemical elements: C in gray, O in magenta, and Ti in pink.

In order to find the most stable adsorption configuration of each nucleobase on the Ti_2CO_2 surface, several initial positions and orientations were tested using the semiempirical extended tight-binding program package (xtb, version 6.2.3) [41,42]. Here, the positions of the surface atoms were fixed, while the atoms of the molecules were free to move to their ground state positions. This initial screening indicated that all five nucleobases prefer to lie parallel to the surface. Thus, the most stable horizontal adsorption configurations were posteriorly fully optimized (i.e., including the MXene surface atoms) at the PBE-D3 level with the VASP code. Despite being less stable than the parallel configurations, the most stable vertical adsorption configuration of each molecule was also studied at the PBE-D3 level, for the sake of comparing the adsorption energy. The adsorption energy, E_{ads}, was calculated as

$$E_{\mathrm{ads}} = E_{\mathrm{mol}*} - (E_* + E_{\mathrm{mol}}) \quad (1),$$

where $E_{\mathrm{mol}*}$, E_*, and E_{mol} are the calculated total energies of a supercell containing a molecule adsorbed on a surface, the pristine surface, and a single molecule, respectively. Thus, adsorption is favorable when E_{ads} is negative and, for each nucleobase, the most stable adsorption configuration is the one with the most negative E_{ads}.

The adsorption configuration of a molecule corresponds to a local minimum of the potential energy landscape when all the Hessian eigenvalues result in real vibrational frequencies for the normal modes of the adsorbed molecule. This verification was carried out by diagonalizing the corresponding block of the Hessian matrix of the system, with elements obtained as finite differences of analytical gradients with displacements widths of 0.015 Å. Since *(i)* the surface-molecule interaction was found to be rather weak —lower than 1 eV—, *(ii)* the surface-molecule distance was high —almost 3 Å—, and *(iii)* the surface atoms practically do not move —at most 0.02 Å—, only the degrees of freedom of the molecule were taken into account in frequency calculations, *i.e.*, they are assumed to be decoupled from the MXene surface phonons.

The effect of the absolute temperature (*T*) and pressure (*p*) on the adsorption stability of the nucleobases was evaluated by calculating the Gibbs free energy of adsorption, G_{ads}, given by

$$G_{\mathrm{ads}} = E_{\mathrm{ads}} - k_{\mathrm{B}} \cdot T \cdot \ln\left(\frac{q_{mol^*}}{q_{mol_{(\mathrm{g})}}}\right) \quad (2).$$

Here, k_{B} is the Boltzmann constant, and q_{mol^*} and $q_{mol_{(\mathrm{g})}}$ are the partition functions of the adsorbed and gas-phase molecule, respectively [43]. In the gas phase, the vibrational, rotational and translation contributions are taken into account [44–46], so that the partition function is $q_{mol_{(\mathrm{g})}} = q_{\mathrm{vib}} \cdot q_{\mathrm{rot}} \cdot q_{\mathrm{trans}} \cdot q_{\mathrm{el}}$, where the electronic contribution, q_{el}, is approximately unitary, given the singlet ground state character of the nucleobases and the large energy difference between their ground state and the excited states. The vibrational contribution is a function of the frequencies, ν_{i}, of the normal vibrational modes, see Table S1 of the Supplementary Data (*SD*), and can be calculated as

$$q_{\mathrm{vib}} = \prod_i \frac{\exp(-h\nu_{\mathrm{i}}/(2k_{\mathrm{B}}T))}{1-\exp(-h\nu_{\mathrm{i}}/(k_{\mathrm{B}}T))} \quad (3),$$

where h is the Planck constant, while the rotational and translational partition functions [43,47] are

$$q_{\mathrm{rot}} \approx \frac{\sqrt{\pi}}{\sigma}\sqrt{\frac{T^3}{\Theta_{r,x}\,\Theta_{r,y}\,\Theta_{r,z}}} \quad (4),$$

and

$$q_{\mathrm{trans}} = \left(\frac{2\pi m k_{\mathrm{B}} T}{h^2}\right)^{3/2}\frac{k_{\mathrm{B}} T}{p} \quad (5),$$

respectively. The quantity σ is the rotational symmetry number which, for all molecules of symmetry C_1 and C_{1h}, as is the case of the nucleobases, is one ($\sigma = 1$) [48]. The $\Theta_{r,i}$ factors are characteristic rotational temperatures of each molecule around the i axes [49], m is the mass of the molecule, and p is the partial pressure of the molecule in the gas phase. The temperature and pressure were fixed at the standard conditions of 298.15 K and 1 bar, respectively, and the rotational temperatures of each molecule were calculated from the diagonalization of the corresponding tensor. The procedure for obtaining the molecular partition functions is the same as the one employed in recent studies [14]. When adsorbed, only the vibrational degrees of freedom need to be considered.

Charge transfer between the Ti_2CO_2 surface and each adsorbed nucleobase was also analyzed by calculating Bader charges [50] and spatial charge density differences between the Ti_2CO_2+nucleobase system and the two isolated components with atomic positions fixed to those of the adsorbed state.

Results

The calculated most stable adsorption configuration of each nucleobase on the Ti_2CO_2 MXene surface is shown in Fig. 2. All the nucleobases prefer to adsorb parallel to the surface. In their adsorbed configurations, the aromatic rings of G and U appear perfectly parallel to the surface, while in the others, especially T, these are slightly tilted. From the top views, one readily concludes that, in all cases, the pyrimidine-like aromatic ring adsorbs approximately centered on a surface oxygen atom and, on A and G, the second ring also attempts to align its center with a nearby oxygen atom of the surface. This tendency to align the aromatic rings with surface oxygens is especially noticeable on the adsorption configuration of U, which is the most symmetric nucleobase. The side views show that the atom closest to the surface is a hydrogen, either from a CH_3 or a NH_2 group, when these are present, or an oxygen atom, in the case of U. The adsorption occurs with the nearest atom sitting more than 2 Å away from the substrate, which presents no visible structural deformation. Non-parallel adsorption is also possible, but metastable, with instability supported by the fact that some of the atomic position optimizations that were performed, using initial perpendicular configurations, yielded parallel configurations instead. For each nucleobase, the most stable non-parallel adsorption configuration is almost perpendicular, and is shown in Fig. S1 of the SD.

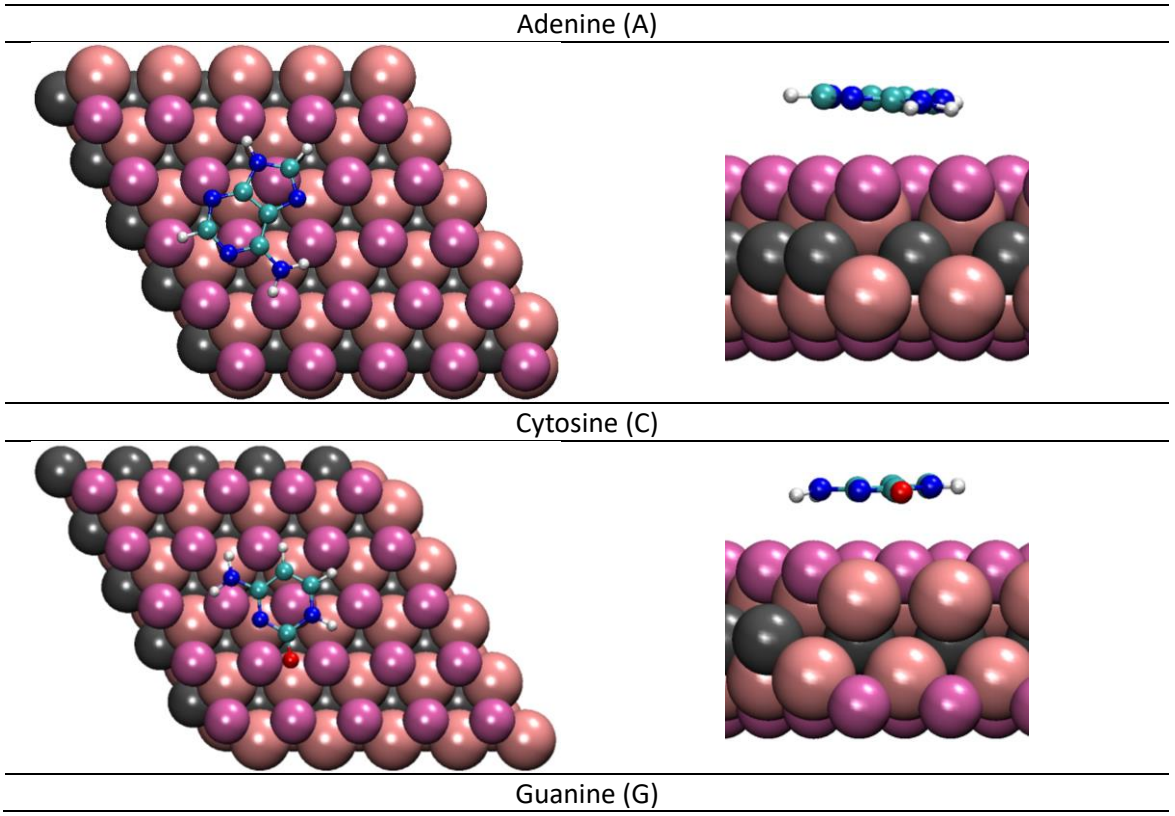

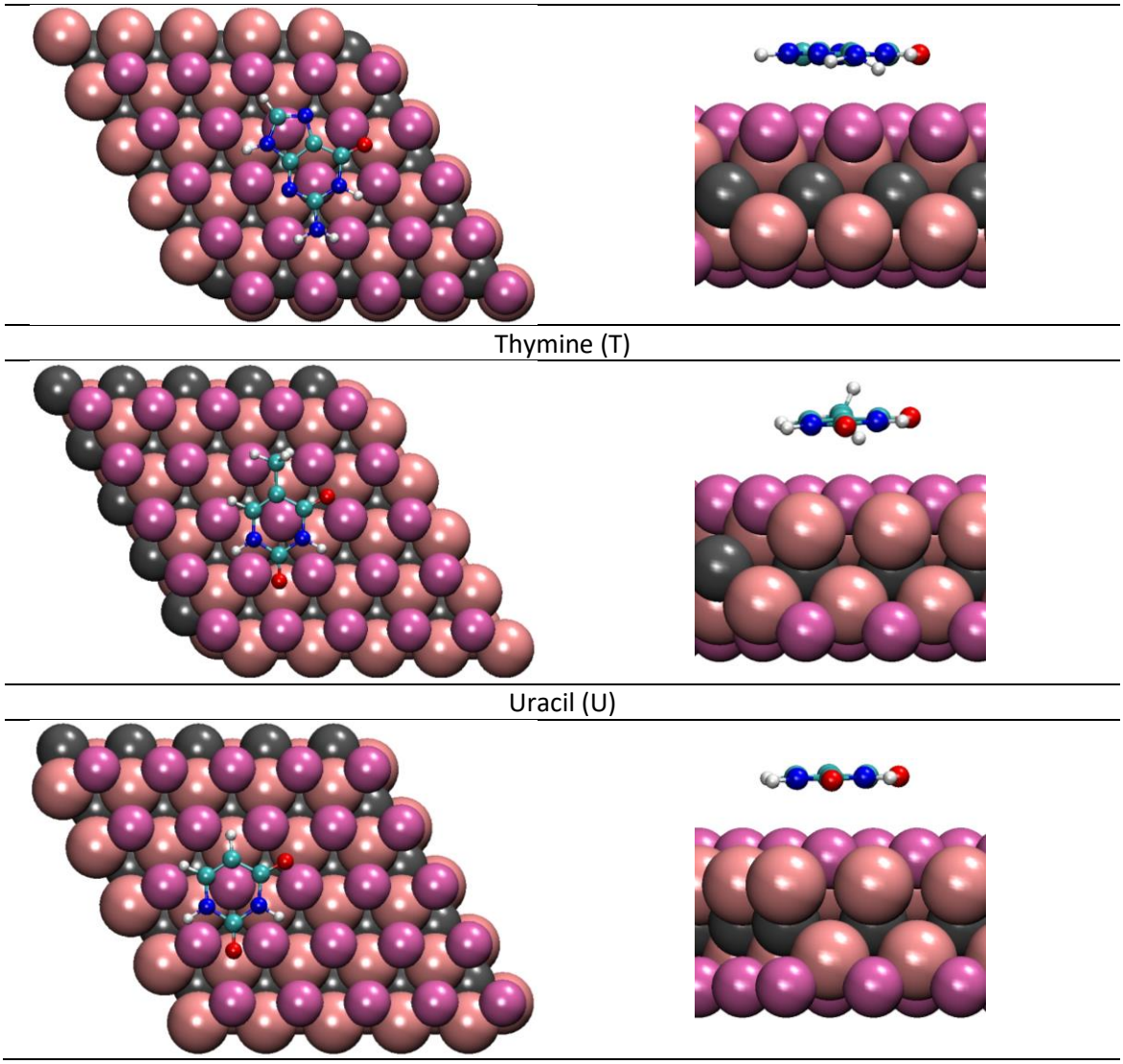

Fig. 2. Top (left images) and side (right images) views of the most stable adsorbed configurations of the five nucleobases on Ti_2CO_2. The color code for the MXene surface atoms is the same as in Figure 1 while, for the atoms of the adsorbates, C is shown in cyan, H in white, N in blue, and O in red.

The adsorption energies of the nucleobases on Ti_2CO_2, among other relevant calculated adsorption-related physicochemical quantities, are shown in Table 1. The nucleobase-MXene distances, measured in the direction perpendicular to the plane of the surface, are of the same order for all molecules, around 2.5 Å. The adsorption energies are all negative, indicating thermodynamically favorable adsorption. The moderate binding energies, close to -1 eV, suggest the molecules are physisorbed. To support this conclusion, we calculated, for each adsorbed nucleobase, the bond orders between all atoms of the molecule and the nearest surface atoms, using the DDEC6 method introduced in Ref. [51]. The highest value found this way corresponds to a carbon atom of G, displaying a bond of order 0.04 with a nearby surface oxygen atom. This is clearly not the order of magnitude expected for a chemical bond, which occurs, for instance, between the same carbon atom and the three nearest (molecular) atoms, with bond orders 1.71, 1.39, and 0.83. We investigated the effect of the adsorption process on the density of states (DOS) of the surface. Plots of the total DOS of the

bare surface, and of the projected DOS of the surface with a G or U molecule adsorbed (the ones with strongest and weakest adsorption strength, respectively), are shown in Fig. S2. The plots are qualitatively and quantitatively very similar, as anticipated for a weak interaction, and as desired for effective preservation of the sensing surface. The absolute values of the parallel adsorption energies are considerably higher, by at least 0.25 eV, than those of perpendicular adsorption. At a temperature of 298.15 K and pressure of 1 bar, the Gibbs free energies of adsorption are also negative for parallel adsorption, while perpendicular adsorption can be endothermic by up to 0.24 eV. For the sake of comparison, we repeated the parallel adsorption calculations, including an implicit solvation model, better mimicking realistic conditions, as implemented in VASPsol [52,53]. The ensuing adsorption configurations remained practically unchanged, while the adsorption became weaker by 0.10 eV on average (see Table 1).

Table 1. Relevant physicochemical quantities for the adsorption of nucleobases on Ti_2CO_2: distance between the MXene oxygen layer and the nearest molecular atom (d), adsorption energy when the molecule adsorbs parallelly ($E_{\mathrm{ads}}^{\mathrm{par}}$) or perpendicularly to the surface ($E_{\mathrm{ads}}^{\mathrm{perp}}$), Gibbs free energy of parallel and perpendicular adsorption ($G_{\mathrm{ads}}^{\mathrm{par}}$ and $G_{\mathrm{ads}}^{\mathrm{perp}}$, respectively) at 298 K and 1 atm, and variation of the Bader charge (ΔQ) of each molecule upon parallel adsorption. The van der Waals volume of each nucleobase (V) is taken from Ref. [54] and the $E_{\mathrm{ads}}^{\mathrm{par}}$ values in parenthesis were calculated using an implicit solvation formalism.

Nucleobase	V (Å^3)	d (Å)	$E_{\mathrm{ads}}^{\mathrm{par}}$ (eV)	$E_{\mathrm{ads}}^{\mathrm{perp}}$ (eV)	$G_{\mathrm{ads}}^{\mathrm{par}}$ (eV)	$G_{\mathrm{ads}}^{\mathrm{perp}}$ (eV)	ΔQ (e)
Adenine	110.42	2.53	-0.84 (-0.75)	-0.54	-0.23	0.00	-0.13
Cytosine	93.32	2.55	-0.81 (-0.65)	-0.55	-0.26	+0.24	-0.07
Guanine	118.77	2.27	-0.97 (-0.90)	-0.68	-0.36	-0.11	-0.21
Thymine	105.10	2.34	-0.80 (-0.71)	-0.51	-0.29	0.00	-0.04
Uracil	88.53	2.67	-0.68 (-0.57)	-0.43	-0.15	+0.08	-0.03

The apparent van der Waals-driven adsorption and the tendency for larger nucleobases to adsorb more strongly hint towards a possible correlation between van der Waals volumes and energies of adsorption. Indeed, these two properties display a squared linear correlation coefficient of $R^2 = 0.83$, as shown in Fig. 3 ($R^2 = 0.93$ in the case of the calculations considering implicit solvent, not shown). However, the Gibbs free energy of adsorption does not correlate as well with the van der Waals volumes, with an $R^2 = 0.62$. The slope of the E_{ads} regression line is about 1.5 times that of G_{ads}, indicating that V has a stronger effect on the adsorption strength at lower temperatures, which, apparently, gets diluted by entropy effects, which are increased by the adsorption-hindered vibrations and are accounted for *via* the Gibbs free energy of adsorption. The difference between the quality of fit when using the adsorption energies and the Gibbs free energies is likely to be simply due to the method of calculation of van der Waals volumes used in the reference from which we took the values. Indeed, although different methods of calculation produce van der Waals volumes of the same order, they can differ by at least as much as 10% (see, for instance, the comparison made in Ref. [55]). Note that the values from Ref. [54] were calculated from the ground state conformation of the nucleobases optimized at zero temperature.

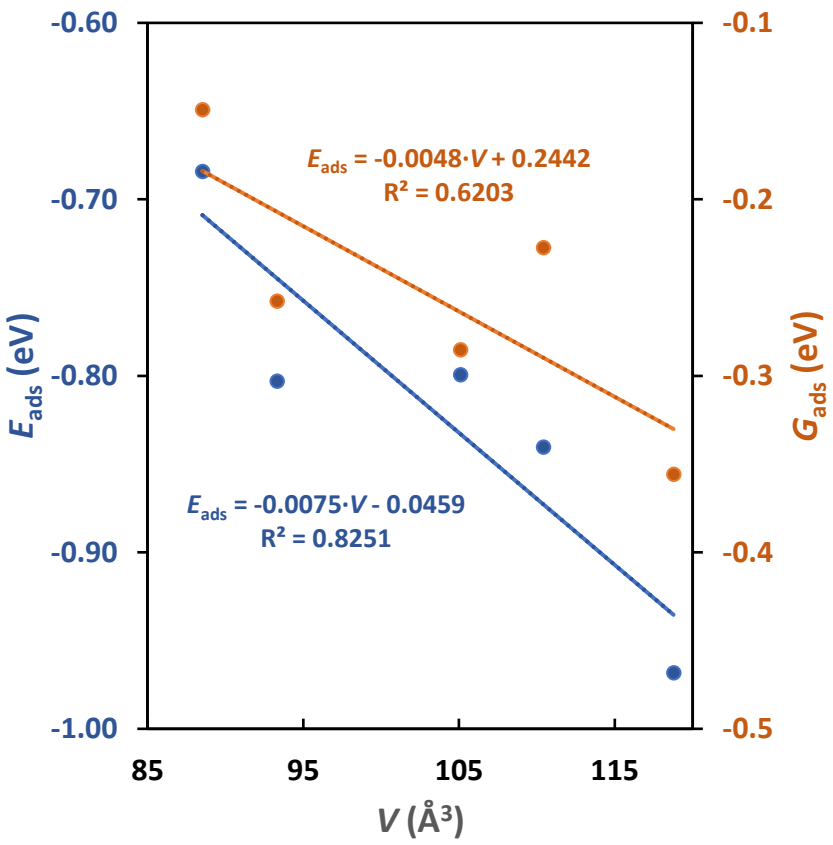

Fig. 3. Calculated adsorption energies (E_{ads}, blue) and Gibbs free energies of adsorption (G_{ads}, orange) of the five nucleobases on the Ti_2CO_2 MXene surface, plotted as a function of their van der Waals volumes (V). The corresponding linear regression lines are also shown, within the same color scheme.

Upon adsorption of a nucleobase, an electron transfer could take place between the MXene surface and the adsorbed molecule. The amount of charge transferred can be evaluated by comparing the total charge of the molecule in gas phase, which is always zero, and the total charge in the adsorbed molecule as estimated by the Bader analysis. In short, Bader's method for dividing molecules into atoms uses the electronic density to estimate the volume occupied by each atom and, from this, the total electronic charge of the atom. By summing over all atoms of a molecule, one obtains its total Bader charge. Finally, the difference between the total Bader charge of the adsorbed molecule, and its isolated form, provides information on how much charge was transferred to or from the surface. These differences (ΔQ), in units of electrons, are shown in Table 1. The negative values displayed signify loss of electrons on the part of the molecule and, therefore, charge transference from the molecule to the MXene surface, which could be detected as an increase of current through an MXene-based sensor. The absolute values of the charge transfer are 0.03 and 0.21, with a clear separation between two groups of molecules: *(i)* those with two aromatic rings, with stronger adsorption and charge transfers above 0.1 electrons, and *(ii)* those with one aromatic ring, displaying weaker adsorption and charge transfers below 0.1 electrons. The values obtained for ΔQ are relatively small, as expected for adsorption phenomena on oxygen-terminated MXenes, which are significantly less reactive than their bare (deoxidized)

counterparts [19]. In order to visually represent the relocation of charge on the molecule and on the surface due to the presence of each other, one can plot isosurfaces of charge density and overlap them with the atomic structure adsorption configurations. This is shown in Fig. 4 for all the nucleobases. The green meshes around the atoms of the molecules, signifying decreases in charge density, generally occupy a larger volume than the grey ones, implying a charge accumulation. Thus, these pictures reflect the aforementioned charge transfer from the molecule to the surface. This is especially evident on adenine and guanine, *i.e.* the nucleobases whose charge transfer is highest.

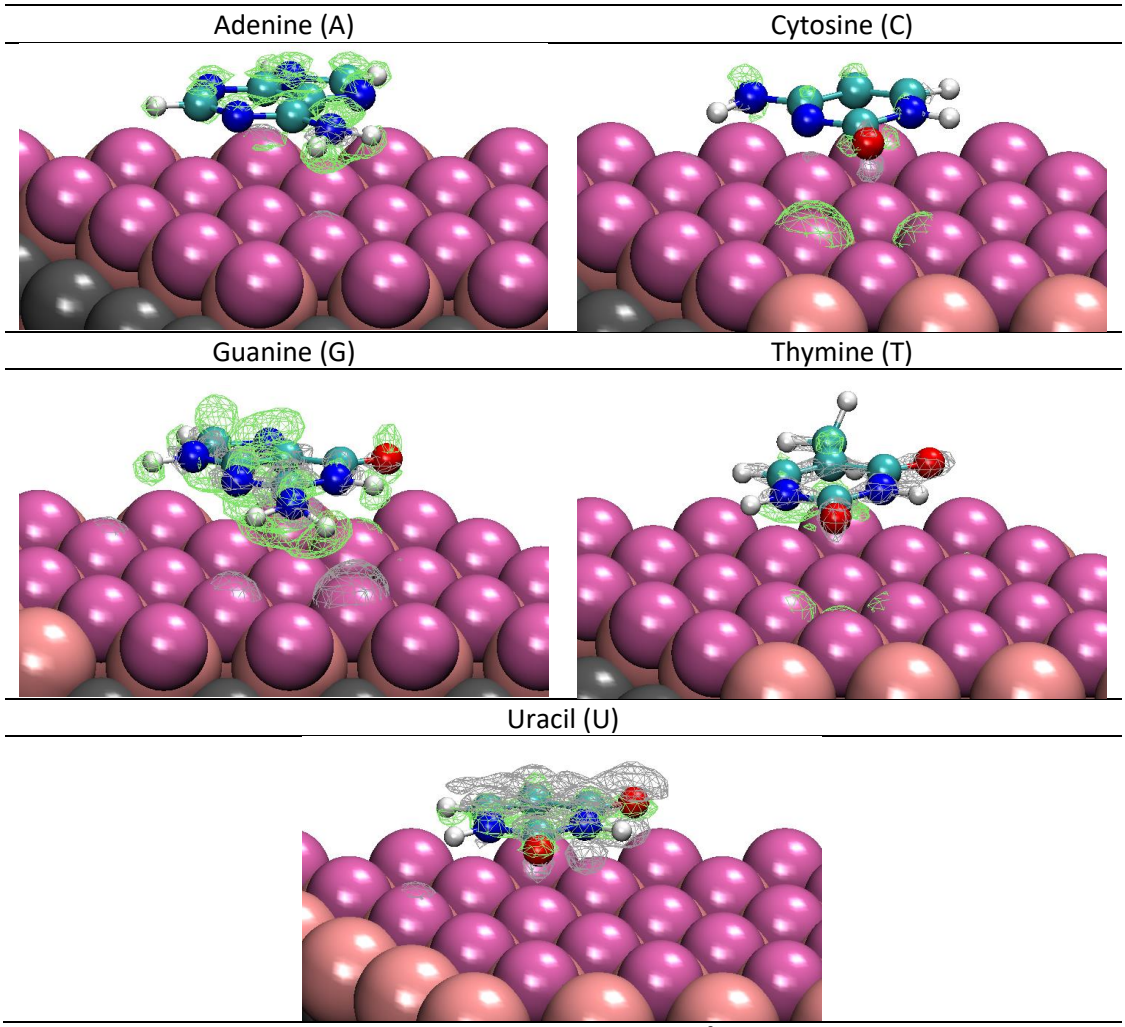

Fig. 4. Electronic density difference isosurfaces (0.005 $e \cdot \text{Å}^{-3}$) for the nucleobases adsorbed onto a Ti_2CO_2 MXene surface. The spheres represent atoms of elements as per the color code in Fig. 2. The green and grey meshes represent decreases or increases of charge density, respectively, with respect to the isolated adsorbate and adsorbent.

Given the above analysis, one should compare the present results to those of similar works. One of our previous studies focused on amino acid adsorption on Ti_2CO_2 [19]. One key resulting qualitative difference is that amino acids have two competing adsorption configurations on Ti_2CO_2: a parallel adsorption configuration, and a tilted one (where the N atom of the amine group bonds with a surface Ti). The adsorption energies corresponding to

these two configurations differ by a few tens of eV on some amino acids, and by at most 0.15 eV on others. On the other hand, our calculations predict that all nucleobases prefer the parallel adsorption by at least 0.25 eV. Most likely, this follows from the fact that the nucleobases contain aromatic rings with a concomitant large contribution of dispersion to the overall interaction. This is at variance with the case of amino acids where the amine group is more clearly separated from the other moieties, and is allowed to form a more directional chemical bond with the surface, strengthening the adsorption. The ranges of adsorption energy values found in both works are, however, very similar and display a reasonable correlation with the van der Waals volume of the molecules. Using the linear regression parameters found in our previous work on adsorption of amino acids to predict the adsorption energies of the nucleobases, we found that the resulting values are off by at most 0.06 eV when compared to the values in Table 1, implying that van der Waals volumes seem to be a general factor determining the interaction of such biological molecules on a Ti_2CO_2 (0001) surface, and, probably, a similar behavior on other MXenes is to be expected.

The adsorption values and mechanisms that result from our calculations are similar to those of the majority of the most recent studies of nucleobase adsorption on two-dimensional substrates. In particular, as seen in Table 2, the adsorption energies found here for Ti_2CO_2 follow the same trend as on MoS_2, boron sheets, penta-graphene, and tellurene [21–23,25,26]. On all of these surfaces, the adsorption energies are sorted in the same order as the van der Waals volumes of the nucleobases, except for C and T. On lithium-doped MoS_2 and silicon nanoribbons, several nucleobases form chemical bonds with the surface and display absolute adsorption energies stronger than -1 eV. This is often considered to render these materials unsuited for sensing purposes due to surface poisoning issues. Overall, our results place Ti_2CO_2 on par with some of the most recently proposed nucleobase sensing surfaces, displaying adsorption energies and charge transfers high enough to be detected, but not so high that they cause the nucleobases to bind too strongly to the MXene and prevent it from being viable as a reusable sensor. Furthermore, the variety and versatility of MXenes, whose composition can be defined by the employed metal, M, the X element, the number of layers, etc., allows for the tuning of MXene-based sensors so as to maximize the sensitivity towards nucleobases in general, a certain type of them, or even specific molecules.

Table 2. Adsorption energies, in eV, of the nucleobases on several selected surfaces. The surfaces shown are, from left to right, the three-layer titanium carbide MXene (Ti_2CO_2) studied in the present work, molybdenum disulfide (MoS_2) [21], lithium-doped MoS_2 (Li-MoS_2) [21], boron surface (B-sheet) [22], penta-graphene (PG) [23], a silicene nanoribbon (Si NR) [24], tellurene (Te) [25], and germanane [27]. For each surface, the background color ranges from green to red, denoting the weakest and strongest nucleobase adsorptions, respectively.

Nucleobase	Ti_2CO_2	MoS_2	Li-MoS_2	B-sheet	PG	Si NR	Te	Ge
Adenine	-0.84	-0.78	-1.55	-0.85	-0.91	-0.67	-0.77	-0.64
Cytosine	-0.81	-0.77	-1.80	-0.73	-0.89	-1.47	-0.72	-0.84
Guanine	-0.97	-0.82	-1.47	-0.99	-1.02	-1.29	-0.95	-1.04
Thymine	-0.80	-0.75	-1.71	-0.78	-0.77	-0.86	-0.66	-1.25
Uracil	-0.68	-0.73	-1.58	---	-0.51	---	-0.60	-1.17

Conclusions

In the present work, we studied, by using state-of-the-art DFT-based methods on proper terminated MXene models, the adsorption of nucleobases on the Ti_2CO_2 MXene case. Qualitatively, we found that all of the examined molecules prefer the adsorption parallel to the surface, with the pyrimidine-like aromatic ring approximately centered on a surface oxygen atom. Neither the molecules nor the surface present any visible structural deformation. Quantitatively, our calculations predict that the adsorbed nucleobases sit around 2.5 Å away from the MXene. The calculated adsorption energy values are all negative, indicating favorable yet moderate adsorption, between -0.68 and -0.97 eV. The adsorption energies display a reasonable correlation with the van der Waals volumes of the molecules. This, along with the small Bader charge differences, between -0.03 and -0.21 *e*, suggests the occurrence of a physisorption with a slight, yet noticeable charge transfer. This conclusion is both in line with previous studies concerning nucleobase adsorption on other stable, not highly reactive surfaces. The predicted properties suggest that this MXene can be employed to develop nucleobase sensors, opening the door to future studies adapting the MXene composition and termination so as to maximize nucleobase sensitivity.

Acknowledgements

The research carried at the University of Aveiro was developed within the scope of the project CICECO-Aveiro Institute of Materials, Refs. UIDB/50011/2020 and UIDP/50011/2020, financed by national funds through the Fundação para a Ciência e a Tecnologia (FCT/MCTES) and co-financed by FEDER under the PT2020 Partnership Agreement. DG is thankful to project SILVIA with reference CENTRO-01-0145-FEDER-31002. The research carried out at the *Universitat de Barcelona* was supported by the Spanish *Ministerio de Ciencia, Innovacion y Universidades* (MICIUN) through the Excellence *María de Maeztu* MDM-2017-0767 and RTI2018-095460-B-I00 grants which involve FEDER funds. Partial support from *Generalitat de Catalunya* (2017SGR13 grant) is also acknowledged. F.I. acknowledges additional support from the 2015 ICREA Academia Award for Excellence in University Research.

References

[1] M. Cox, D.L. Nelson, Lehninger Principles of Biochemistry, Fourth edition. New York : W.H. Freeman, 2005., 2008.

[2] M. Naguib, M. Kurtoglu, V. Presser, J. Lu, J. Niu, M. Heon, L. Hultman, Y. Gogotsi, M.W. Barsoum, Adv. Mater. 23 (2011) 4248–4253.

[3] J. Peng, X. Chen, W.J. Ong, X. Zhao, N. Li, Chem 5 (2019) 18–50.

[4] B. Anasori, M.R. Lukatskaya, Y. Gogotsi, Nat. Rev. Mater. 2 (2017) 16098.

[5] H. Wang, Y. Wu, X. Yuan, G. Zeng, J. Zhou, X. Wang, J.W. Chew, Adv. Mater. 30 (2018) 1704561.

[6] Q. Jiang, N. Kurra, M. Alhabeb, Y. Gogotsi, H.N. Alshareef, Adv. Energy Mater. 8 (2018) 1703043.

[7] M. Naguib, J. Come, B. Dyatkin, V. Presser, P.L. Taberna, P. Simon, M.W. Barsoum, Y. Gogotsi, Electrochem. Commun. 16 (2012) 61–64.

[8] X. Yu, Y. Li, J. Cheng, Z. Liu, Q. Li, W. Li, X. Yang, B. Xiao, ACS Appl. Mater. Interfaces 7 (2015) 13707–13713.

[9] R. Morales-Salvador, Á. Morales-García, F. Viñes, F. Illas, Phys. Chem. Chem. Phys. 20 (2018) 24490–24493.

[10] I. Persson, J. Halim, H. Lind, T.W. Hansen, J.B. Wagner, L.-Å. Näslund, V. Darakchieva, J. Palisaitis, J. Rosen, P.O.Å. Persson, Adv. Mater. 31 (2019) 1805472.

[11] Á. Morales-García, A. Fernández-Fernández, F. Viñes, F. Illas, J. Mater. Chem. A 6 (2018) 3381–3385.

[12] L.M. Azofra, N. Li, D.R. MacFarlane, C. Sun, Energy Environ. Sci. 9 (2016) 2545–2549.

[13] J.D. Gouveia, Á. Morales-García, F. Viñes, F. Illas, J.R.B. Gomes, Appl. Catal. B Environ. 260 (2020) 118191.

[14] J.D. Gouveia, Á. Morales-García, F. Viñes, J.R.B. Gomes, F. Illas, ACS Catal. 10 (2020) 5049–5056.

[15] F. Vitale, N. Driscoll, B. Murphy, in: B. Anasori, Y. Gogotsi (Eds.), 2D Met. Carbides Nitrides Struct. Prop. Appl., Springer International Publishing, Cham, 2019, pp. 503–524.

[16] M. Long, H.. Rack, Biomaterials 19 (1998) 1621–1639.

[17] W. Liu, S. Xu, B. Hu, X. Wang, Proc. IEEE Int. Conf. Micro Electro Mech. Syst. 2018-Janua (2018) 348–351.

[18] M. Mojtabavi, A. VahidMohammadi, W. Liang, M. Beidaghi, M. Wanunu, ACS Nano 13 (2019) 3042–3053.

[19] J.D. Gouveia, G. Novell-Leruth, P.M.L.S. Reis, F. Viñes, F. Illas, J.R.B. Gomes, ACS Appl. Bio Mater. 3 (2020) 5913–5921.

[20] P. Urbankowski, L. Miao, J. Jiang, C. Chen, M. Boota, B. Anasori, Y. Gogotsi, J. Mater. Chem. A (2018) 4617–4622.

[21] M. Sadeghi, M. Jahanshahi, M. Ghorbanzadeh, G. Najafpour, Appl. Surf. Sci. 434 (2018) 176–187.

[22] A. Sihag, S.S. Mallajosyula, ChemistrySelect 4 (2019) 3308–3314.

[23] B. Li, Z.-G. Shao, Appl. Surf. Sci. 512 (2020) 145635.

[24] Q. Li, H. Liu, Y. Tian, J. Guo, G. Chen, J.Y. Lee, J. Phys. Chem. C 124 (2020) 10823–10831.

[25] H. Guo, K. Zheng, H. Cui, J. Yu, L.-Q. Tao, X. Li, C. Liao, L. Xie, X. Chen, Appl. Surf. Sci. 532 (2020) 147451.

[26] H. Yang, Y. Liu, C. Gao, L. Meng, Y. Liu, X. Tang, H. Ye, J. Phys. Chem. C 123 (2019) 30949–30957.

[27] U. Srimathi, V. Nagarajan, R. Chandiramouli, Comput. Theor. Chem. 1130 (2018) 68–76.

[28] C. Chen, M. Boota, P. Urbankowski, B. Anasori, L. Miao, J. Jiang, Y. Gogotsi, J. Mater. Chem. A 6 (2018) 4617–4622.

[29] P. Singla, M. Riyaz, S. Singhal, N. Goel, Phys. Chem. Chem. Phys. 18 (2016) 5597–5604.

[30] G. Kresse, J. Hafner, Phys. Rev. B 47 (1993) 558–561.

[31] G. Kresse, J. Hafner, Phys. Rev. B 49 (1994) 14251–14269.

[32] G. Kresse, J. Furthmüller, Phys. Rev. B 54 (1996) 11169–11186.

[33] G. Kresse, J. Furthmüller, Comput. Mater. Sci. 6 (1996) 15–50.

[34] J.P. Perdew, K. Burke, M. Ernzerhof, Phys. Rev. Lett. 77 (1996) 3865–3868.

[35] S. Grimme, J. Antony, S. Ehrlich, H. Krieg, J. Chem. Phys. 132 (2010) 154104.

[36] S. Grimme, S. Ehrlich, L. Goerigk, J. Comput. Chem. 32 (2011) 1456–1465.

[37] J.P.P. Ramalho, J.R.B. Gomes, F. Illas, RSC Adv. 3 (2013) 13085.

[38] F. Viñes, O. Lamiel-García, J. Phys. Chem. C 123 (2019) 11714–11722.

[39] L. Vinet, A. Zhedanov, J. Phys. A Math. Theor. 44 (2011) 085201.

[40] N. Zhang, Y. Hong, S. Yazdanparast, M. Asle Zaeem, 2D Mater. 5 (2018) 045004.

[41] S. Grimme, C. Bannwarth, P. Shushkov, J. Chem. Theory Comput. 13 (2017) 1989–2009.

[42] C. Bannwarth, S. Ehlert, S. Grimme, J. Chem. Theory Comput. 15 (2019) 1652–1671.

[43] Keith J Laidler, Chemical Kinetics, 3rd ed., Harper Collins, New York, 1987.

[44] M.A.O. Lourenço, P. Ferreira, J.R.B. Gomes, Phys. Chem. Chem. Phys. 20 (2018) 16686–16694.

[45] C. Kunkel, F. Viñes, F. Illas, Energy Environ. Sci. 9 (2016) 141–144.

[46] C. Kunkel, F. Viñes, M.A.O. Lourenço, P. Ferreira, J.R.B. Gomes, F. Illas, Chem. Phys. Lett. 671 (2017) 161–164.

[47] D.A. McQuarrie, Statistical Mechanics, Harper & Row, New York, 1975.

[48] G. Herzberg, Molecular Spectra and Molecular Structure II: Infrared and Raman of Polyatomic Molecules, Van Nostrand, New York, 1956.

[49] P.W. Atkins, J. De Paula, Atkins' Physical Chemistry, Oxford Univ. Press, Oxford, 2006.

[50] G. Henkelman, A. Arnaldsson, H. Jónsson, Comput. Mater. Sci. 36 (2006) 354–360.

[51] T.A. Manz, RSC Adv. 7 (2017) 45552–45581.

[52] K. Mathew, R. Sundararaman, K. Letchworth-Weaver, T.A. Arias, R.G. Hennig, J. Chem. Phys. 140 (2014) 084106.

[53] K. Mathew, V.S.C. Kolluru, S. Mula, S.N. Steinmann, R.G. Hennig, ArXiv (2016).

[54] S.-C. Yam, S.M. Zain, V. Sanghiran Lee, K.-H. Chew, Eur. Phys. J. E 41 (2018) 86.

[55] Y.H. Zhao, M.H. Abraham, A.M. Zissimos, J. Org. Chem. 68 (2003) 7368–7373.